Solar Energy Materials and Solar Cells 173 (2017) 111–119

Contents lists available at ScienceDirect

Solar Energy Materials and Solar Cells

journal homepage: www.elsevier.com/locate/solmat

Atomic layer deposition of high-mobility hydrogen-doped zinc oxide

Bart Macco[a,*], Harm C.M. Knoops[a,b], Marcel A. Verheijen[a], Wolfhard Beyer[c], Mariadriana Creatore[a,d], Wilhelmus M.M. Kessels[a,d]

[a] Department of Applied Physics, Eindhoven University of Technology, P.O. Box 513, 5600 MB Eindhoven, The Netherlands
[b] Oxford Instruments Plasma Technology, North End, Bristol BS49 4AP, UK
[c] IEK-5, Forschungszentrum Jülich, 52428 Jülich, Germany
[d] Solliance Solar Research, High Tech Campus 5, 5656 AE Eindhoven, The Netherlands

ARTICLE INFO

Keywords:
Atomic layer deposition
Transparent conductive oxide
Spectroscopic ellipsometry
Carrier mobility
Hydrogen doping
Zinc oxide

ABSTRACT

In this work, atomic layer deposition (ALD) has been employed to prepare high-mobility H-doped zinc oxide (ZnO:H) films. Hydrogen doping was achieved by interleaving the ZnO ALD cycles with H2 plasma treatments. It has been shown that doping with H_2 plasma offers key advantages over traditional doping by Al and B, and enables a high mobility value up to 47 cm^2/Vs and a resistivity of 1.8 mΩcm. By proper choice of a deposition regime where there is a strong competition between film growth and film etching by the H2 plasma treatment, a strongly enhanced grain size and hence increased carrier mobility with respect to undoped ZnO can be obtained. The successful incorporation of a significant amount of H from the H_2 plasma has been demonstrated, and insights into the mobility-limiting scatter mechanisms have been obtained from temperature-dependent Hall measurements. A comparison with conventional TCOs has been made in terms of optoelectronic properties, and it has been shown that high-mobility ZnO:H has potential for use in various configurations of silicon heterojunction solar cells and silicon-perovskite tandem cells.

1. Introduction

Thin films of transparent conductive oxides (TCOs) are commonly used as transparent electrodes in a wide range of solar cell architectures, such as silicon heterojunction (SHJ), Copper indium gallium selenide (CIGS), and perovskite solar cells. Often-employed TCO materials are based on indium oxide (In_2O_3), zinc oxide (ZnO) and tin oxide (SnO_2). Ideally, such TCO layers are both highly conductive and optically transparent in order to minimize ohmic and optical losses, respectively. In order to achieve a sufficient level of conductivity, typically on the order of 1 mΩcm or lower, the carrier density in these materials is raised to the order of 10^{19}–10^{20} cm^{-3} by the introduction of n-type dopants, such as Sn in In_2O_3, Al or B in ZnO and F in SnO_2. However, increasing the conductivity by increasing the carrier density comes at the expense of reduced optical performance: At high carrier densities, the plasma frequency of the TCO enters the near infrared (NIR) range, and the free carriers start to affect the dielectric function in the NIR through the so-called Drude contribution. The extinction coefficient k is increased, leading to free-carrier absorption (FCA), whereas the refractive index n is decreased, leading to a non-ideally matched antireflection coating and thus free-carrier reflection (FCR). This is especially detrimental for solar cells for which the absorber layer has a band gap in the NIR, such as SHJ solar cells. For example, the optical losses induced by free-carrier effects in conventional Sn-doped In_2O_3 (ITO) used as front electrode in SHJ solar cells in terms of photocurrent have been quantified by optical simulations to be around 2.4 mA/cm^2, compared to the 44 mA/cm^2 available in the AM1.5 g spectrum [1]. Because of these adverse effects induced by the free carriers, it is preferred to achieve a high level of conductivity through a high carrier mobility (i.e. low scattering of electrons) rather than through a high density of electrons.

In order to achieve a high mobility, the TCO material must be engineered such that electrons experience as little scattering as possible. In TCO materials there are various scattering mechanisms that play a role. Scattering from phonons and ionized dopants is in a sense unavoidable, and are therefore labelled as *intrinsic* scatter mechanisms. Other scatter mechanisms are related to material quality, and are called *extrinsic* scatter mechanisms. Examples of the latter mechanisms include scattering at grain boundaries, at impurities and at ineffective or clustered dopants. Therefore, the general aim is to mitigate the *extrinsic* scatter mechanisms such that the mobility limit set by the *intrinsic* scatter mechanisms is reached. For the carrier density range of interest of around 10^{20} cm^{-3}, the upper limit for the mobility set by the intrinsic scatter mechanisms is about ~55 cm^2/Vs for ZnO-based and ~130 cm^2/Vs for In_2O_3-based TCOs. [2,3].

In the case of In_2O_3-based TCOs, ITO has historically been the TCO

* Corresponding author.

http://dx.doi.org/10.1016/j.solmat.2017.05.040
Received 10 April 2017; Received in revised form 10 May 2017; Accepted 17 May 2017
Available online 25 May 2017
0927-0248/ © 2017 The Authors. Published by Elsevier B.V. This is an open access article under the CC BY-NC-ND license (http://creativecommons.org/licenses/BY-NC-ND/4.0/).

material of choice. Nonetheless, its typical mobility value of 20–40 cm^2/Vs [4] is well below the mobility limit set by the intrinsic scatter mechanisms. Therefore, in recent years there has been a strong interest in various *high-mobility* In_2O_3-based TCOs which employ novel dopants such as H, W and Mo. [5–8] Especially H-doped In_2O_3 (In_2O_3:H) has been shown to yield record high mobility values of 130 cm^2/Vs, which is as high as the mobility limit [3]. This high-quality material has been prepared both by sputtering [5] and by atomic layer deposition (ALD) [6]. The enhanced mobility lowers the required carrier density to the low 10^{20} cm^{-3} regime, thereby almost completely negating IR-losses and enhancing the J_{sc} of SHJ solar cells when applied as the front electrode [9,10]. The enhanced mobility enabled by the H dopant compared to the traditional Sn dopant is mainly ascribed to two key factors: Firstly, grain boundary scattering has been found to be negligible in H-doped In_2O_3. This has been attributed to the fact that H-doped In_2O_3 has very large grains of a few hundred nanometer. [3,5,6,11] In addition, the grain boundaries are well-passivated by the available H. Secondly, inactive H dopants have been shown to not contribute to electron scattering. [3].

Although such high-mobility In_2O_3-based TCOs yield excellent performance, concerns regarding the scarcity and price of indium are a strong driver to replace In_2O_3-based TCOs with doped ZnO-based TCOs. Despite many efforts, the level of performance in terms of optical transparency and electrical conductivity offered by Al- or B-doped ZnO TCOs is not on par with the In_2O_3-based TCOs. Experimentally-obtained mobility values are typically well below 30 cm^2/Vs. Therefore, keeping the aforementioned mobility limit of ZnO films of ~55 cm^2/Vs in mind, there is a lot of room for improvement of doped ZnO TCOs.

Similar as for In_2O_3, also in the case of ZnO hydrogen has emerged as a very promising alternative dopant. *Ab initio* calculations show that bond-centered (BC) H is the most stable configuration and acts as a shallow donor. [12,13] Experimentally, the beneficial effect of H on ZnO has been reported being either through H being embedded during deposition [14,15], by annealing in H_2 atmosphere [16], or through exposure to H_2 plasma [17,18]. For example, Ding *et al.* showed that mobility values as high as 58 and 46 cm^2/Vs could be obtained for 2 μm and 350 nm thick films by exposing these films to H_2 plasma after deposition. [18] Gaspar *et al.* recently showed that high-mobility ZnO:H can be prepared by the addition of H_2 during rf reactive magnetron sputtering. [19] They achieved an optimized mobility value of 47.1 cm^2/Vs and a carrier density of 4.4×10^{19} cm^{-3}, resulting in a resistivity value of 2.8 mΩ cm. In addition, Thomas *et al.* have shown that ZnO:H can be prepared by ALD. [15] They interleaved standard ALD ZnO cycles comprised of diethylzinc (DEZ, $Zn(C_2H_5)_2$) and H_2O exposures with H_2 plasma exposures, and reached much higher carrier density values of up to 4.6×10^{20} cm^{-3}, respectable mobility values around 20 cm^2/Vs and low resistivity values down to 0.7 mΩcm.

In this work, we employ a process consisting of thermal ALD in conjunction with interleaved H_2 plasma treatments to prepare ZnO:H films, similar to the approach of Thomas *et al.* [15] It will be shown that the H_2 plasma treatment has an etching component that can be employed to strongly enhance the structural and optoelectronic properties of the ZnO:H films. More specifically, by growing ZnO:H films in a regime where film nucleation is in strong competition with etching from the H_2 plasma, a strong enhancement of the grain size and a preferential c-axis orientation can be obtained. Under such conditions, our process results in high-mobility (~47 cm^2/Vs) and conductive (~1.8 mΩcm) ZnO:H with excellent IR-transparency. Furthermore, insights into the doping by the H_2 plasma and into the electron scatter mechanisms in our high-mobility ZnO:H have been obtained from effusion and temperature-dependent Hall measurements, respectively. Finally, the material properties of ALD ZnO:H are compared to conventional TCO materials, and the potential of ALD ZnO:H for the application in various Si solar cell configurations is discussed.

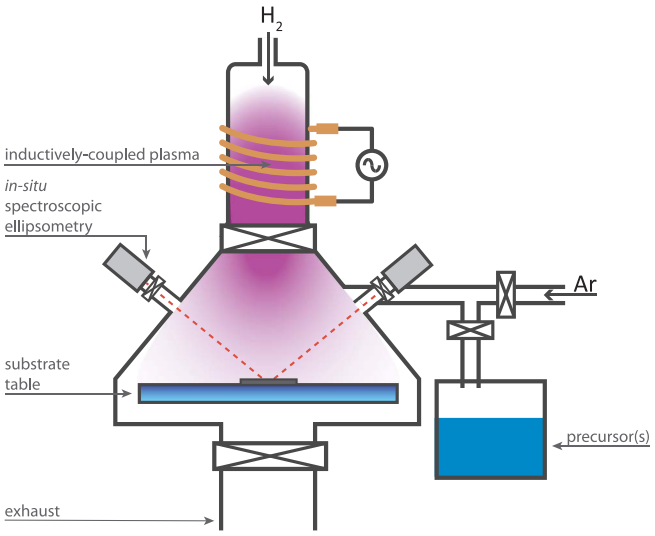

Fig. 1. Schematic of the Oxford Instruments OpAL ALD reactor used in this work. The spectroscopic ellipsometer used for in-situ film thickness determination is shown as well. Note that multiple precursor pots have been used in this work (for DEZ and H_2O), but that only one is shown.

2. Experimental section

Silicon wafers coated with ~430 nm of thermal oxide were used as substrates. ~75 nm thick H-doped ZnO films were deposited in an Oxford Instruments OpAL ALD reactor at a substrate temperature of 200 °C. DEZ and deionized water vapor were used as precursors for ZnO growth. A schematic of the setup is shown in Fig. 1.

H doping was achieved by interleaving H_2 plasma treatments every *n* ALD cycles, in a so-called supercycle fashion as shown in Fig. 2. The integer *n*, i.e. the number of ZnO cycles in between the H_2 plasma treatments, is called the cycle ratio. A remote inductively coupled plasma was used for the H_2 plasma treatment, with a plasma power of 100 W, a H_2 flow of 50 sccm and an exposure time of 4 s being the standard condition.

Film growth was monitored in-situ by spectroscopic ellipsometry (SE). The SE setup used for these measurements is a J. A. Woollam Co. Inc. M-2000D spectrometer with an XLS-100 light source (0.7 − 5.0 eV of photon energy). For analysis of the SE data, the dielectric function of the ALD ZnO:H films was modeled using a combination of a Tauc-Lorentz, Gaussian and Drude oscillator. [20] The electrical properties were determined from Hall measurements (Ecopia HMS-5300 Hall Effect Measurement System). In addition, temperature-dependent Hall measurements down to 80 K were performed using a stage cooled by liquid nitrogen. The surface morphology was evaluated by atomic force microscopy using a NT-MDT Solver P47 microscope in tapping mode

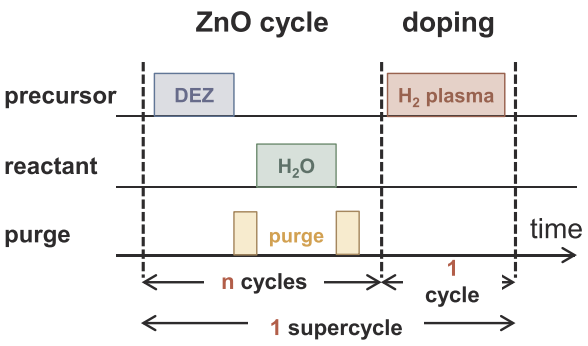

Fig. 2. Schematic of the so-called supercycle approach used to prepare ZnO: H. After *n* cycles of ALD ZnO, the film is exposed to a H_2 plasma treatment. Together, these *n* ZnO cycles and H_2 plasma treatment constitute a supercycle.

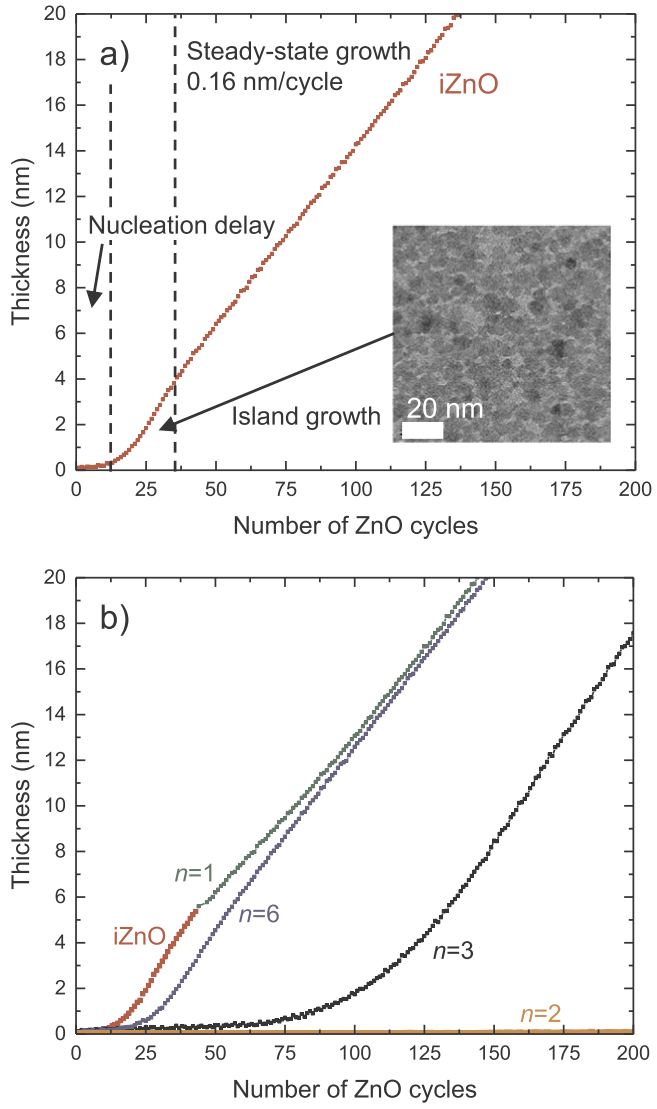

Fig. 3. (a) Growth of an undoped ALD ZnO layer as a function of the number of ZnO cycles. The various stages of growth are indicated. The top-view transmission electron microscopy image in the inset shows the island growth during initial film growth. (b) Growth of ALD ZnO:H layers for varying cycle ratios *n*. In this example, the cycle ratio $n=1$ layer was grown on top of an iZnO seed layer.

using TiN-coated Si tips (NSG10/TiN, NT-MDT). X-ray diffraction measurements were performed using a Panalytical X'Pert PRO MRD employing Cu Kα (1.54 Å) radiation. Transmission electron microscopy (TEM) analysis (JEOL ARM 200 probe corrected TEM, operated at 200 kV) was used to study cross-sections of films using focused ion beam (FIB) made lamellas. Thermal effusion measurements were performed in a high vacuum (7.5×10^{-7} Torr) quartz tube. A linear ramp rate of 20 °C/min was used and the effused H_2 molecules were detected using a quadrupole mass spectrometer (QMS). The H_2 flow was calibrated as described in reference [21].

3. Results and discussion

3.1. Influence of the H_2 plasma treatment on the film growth

The H_2 plasma treatment was found to have a pronounced influence on the film growth, which can be used to strongly improve the properties of the ZnO: H. However, before discussing the influence of the H_2 plasma on the film growth of ZnO: H, it is instructive to first review the different stages of film growth for undoped ZnO by ALD. In Fig. 3(a), a typical growth curve for ALD ZnO is shown. Such a curve is obtained using in-situ SE, where the film thickness is monitored as a function of the number of ALD cycles. As can be seen, the growth is characterized by a short nucleation delay during the first ~10 cycles. This is followed by an island-like growth mode typical of ALD ZnO, as can be seen in the inset top-view transmission electron microscopy image in Fig. 3(a). This growth regime is accompanied by an enhanced growth rate. [22] Afterwards, the islands coalesce and steady–state film growth with a growth per cycle (GPC) of 0.16 nm is obtained.

As will be shown, the H_2 plasma treatment slightly influences the growth of ZnO by etching of the ZnO. Therefore, the etch rate of ZnO films upon extended H_2 plasma exposure in our setup has been studied. This has been done by exposing a 50 nm-thick ZnO sample to H_2 plasma, and monitoring the thickness decrease in real-time by in-situ SE. For our standard plasma condition of 100 W plasma power and 50 sccm of H_2 flow, a etch rate of 0.23 nm/min was found (see Fig. S1 of the Supplementary Information). In the 4 s of H_2 plasma used in the supercycle, it is thus expected that only 0.015 nm is etched. Since this is much less than the steady-state growth-per-cycle (GPC) of 0.16 nm for the ZnO process, a strong etching effect is not to be expected during steady-state growth.

However, the H_2 plasma treatment has been found to strongly influence especially the initial growth during the ALD process. Using in-situ SE, the initial ALD growth has been monitored for various cycle ratios *n*, as shown in Fig. 3(b). When going to cycle ratios $n=6$ and $n=3$, a strong increase in the nucleation delay is observed compared to the case of non-intentionally doped ZnO (iZnO, i.e., no H_2 plasma step is used). This can be understood from the fact that even though the amount of ZnO etched during the H_2 plasma step is much less than the *steady-state* GPC, it can become comparable to the GPC during the nucleation phase of the ZnO layers, which is much lower than the steady-state value. Note that for a cycle ratio of $n=2$, no film growth was observed even after 200 cycles, showing that for such conditions the H_2 plasma is able to prevent film growth altogether. The absence of film growth for such low cycle ratios can be circumvented by first growing a thin seed layer of ~5 nm iZnO, followed by thickening of the film at e.g. a cycle ratio of $n=1$, as can been seen in Fig. 3(b). Throughout this work, several films have been deposited on top of such seed layers. Films grown on a 5 nm iZnO layer are denoted by an asterisk (*). In addition, select films were grown on a 5 nm ZnO:H seed layer which itself was grown using a cycle ratio *n* of 3. These films are denoted by a double asterisk (**).

Besides influencing the initial growth of the film, the H_2 plasma treatment has been found to strongly enhance the grain size. This can be seen from the AFM images in Fig. 4. Going to a cycle ratio of 6 and 3 progressively leads to an enhanced feature size and an increase in film roughness with respect to the iZnO film. From the AFM images a rough estimation of the surface grain size has been made by manual counting of the areal grain density. Values of approximately 50, 85 and 110 nm have been obtained for the iZnO, $n=6$ and $n=3$ films, respectively. Interestingly, a film comprised of a 5 nm iZnO seed layer which is subsequently thickened with a process using $n=3$ has a strongly reduced feature size compared to the $n=3$ film grown without a seed layer (Fig. 4(c) and (d)), and a grain size of 50 nm has been estimated for this film, similar to that of the iZnO film.

The increase in grain size with decreasing cycle ratio *n* is thought to originate from etching of the ZnO layer by the H_2 plasma during the nucleation of the film. At low cycle ratio *n*, more nuclei are etched during the initial stages of growth. This reduces the nuclei density, leading to an enhanced grain size. However, when an iZnO seed layer is used, the initial layer has an equally high density of nuclei as when no H_2 plasma is used, explaining the difference between Fig. 4(c) and (d). Note that this enhanced crystal size induced by the H_2 plasma treatment is in strong contrast to Al- and B-doping which leads to interruption of crystal growth and thus a reduced grain size compared to the undoped case [23].

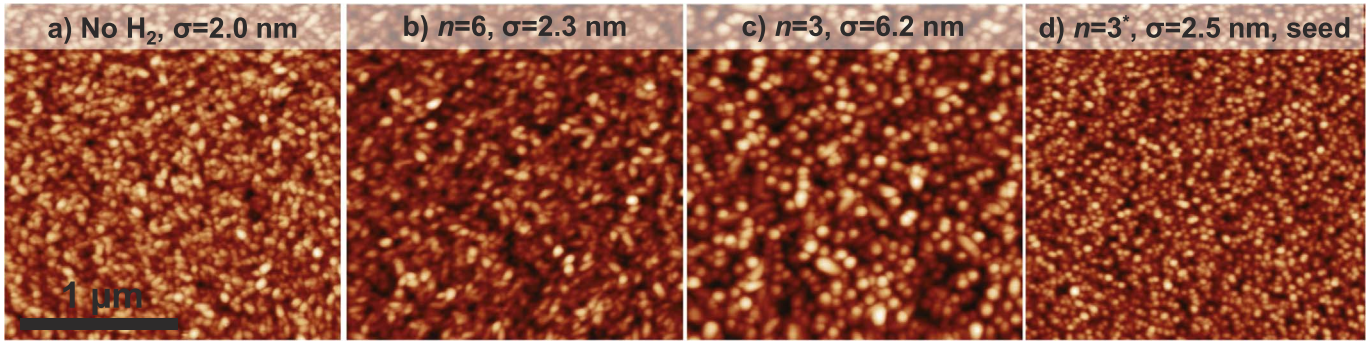

Fig. 4. AFM images of ZnO film grown (a) without H_2 plasma treatment, (b) using a cycle ratio *n* of 6, (c) using a cycle ratio *n* of 3, and (d) using a cycle ratio *n* of 3 on top of a 5 nm iZnO seed layer. The root mean square roughness *σ* is given.

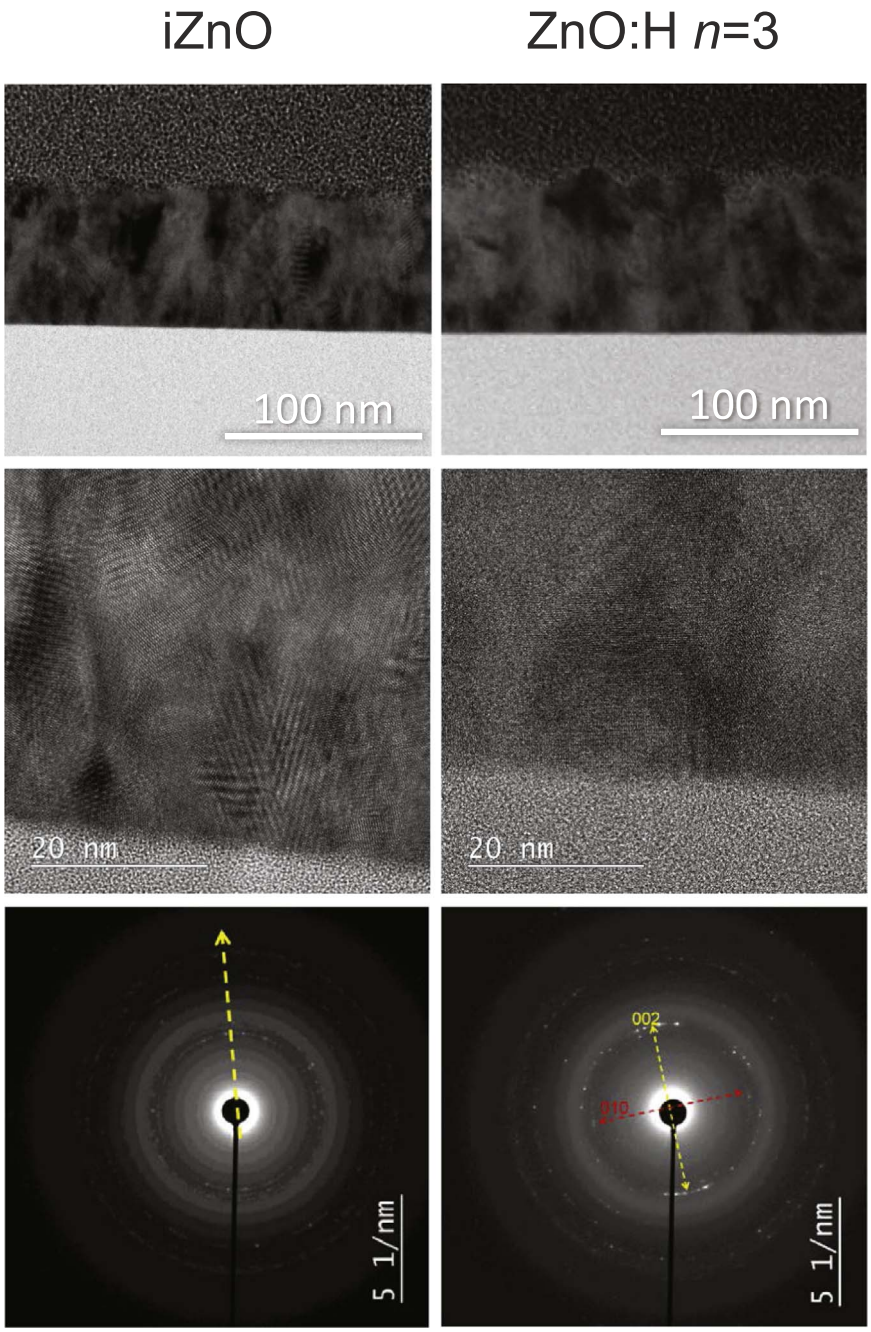

Fig. 5. Cross-sectional TEM images (top row), close-up TEM images (middle row) and SAED patterns (bottom row) of (left column) iZnO films grown without H_2 plasma and (right column) ZnO:H films grown using a cycle ratio $n = 3$.

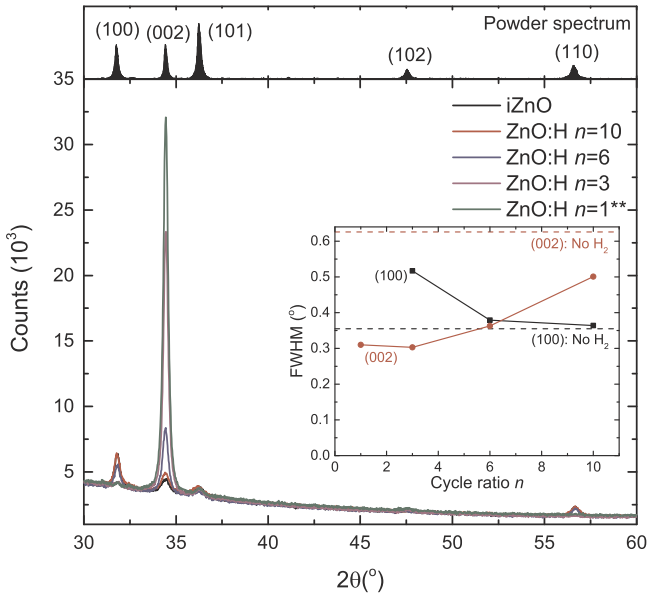

Fig. 6. XRD 2θ scans of ZnO:H films prepared at various cycle ratios *n*. The Miller indices of the diffraction peaks of ZnO are indicated. (Inset) Full width at half maximum (FWHM) of the peaks belonging to the (100) and (002) orientations. The dashed lines show the FWHM values of ZnO films prepared without H_2 plasma treatment. For the $n=1^{**}$ film, no (100) peak was discernable. The top panel shows the powder spectrum of ZnO (RRUFF database, entry R060027.1).

The beneficial effect of the H_2 plasma treatment on the film morphology has been corroborated by cross-sectional TEM. In Fig. 5, a comparison between iZnO and ZnO:H grown with a cycle ratio *n* of 3 is shown. Upon close inspection, three main differences between the two films can be discerned. Firstly, the H-doped sample shows a rougher top surface morphology, in line with the AFM results. Secondly, the H-doped sample features large columnar grains that extend to the film surface, whereas the iZnO has smaller grains with a less prominent structure. Thirdly, when looking at selected area electron diffraction (SAED) patterns in Fig. 5 (acquired from an area containing a 1.3 μm long part of the ZnO layer), the arc segments in the pattern of the doped ZnO sample suggest a < 002 > texture, whereas the continuous rings of the iZnO sample point to a more random crystal orientation.

The change in film crystal morphology induced by the H_2 plasma treatment can also clearly be seen from XRD measurements, as shown in Fig. 6. The iZnO reference sample has dim peaks originating from various orientation, with the (100) direction being the most pronounced. For the powder spectrum of ZnO, shown in the top panel of Fig. 6, the (101) direction has the highest intensity. Therefore, the iZnO has a slight < 100 > texture. For decreasing cycle ratio *n*, a strong increase in the (002) orientation and a decrease in the other orientations is observed, showing that the H_2 plasma treatment induces a strong c-axis < 002 > texture. As shown in the inset of Fig. 6, at the same time the diffraction peak belonging to the (002) orientation becomes narrower, whereas the (100) diffraction peak broadens. This points to an enhanced vertical grain size for the (002) oriented grains, in line with the observed columnar crystal morphology, and a lower vertical grain size for the (100) oriented grains. Interestingly, for the cycle ratio $n=1^{**}$ sample which is prepared on a 5 nm $n=3$ seed layer, the preferred (002) orientation is manifested more strongly compared to the film grown with $n=3$. This suggests that the preferential orientation is not merely determined during the nucleation phase by etching of initial nuclei by the H_2 plasma treatment, but is also influenced by the H_2 plasma during steady-state film growth. It should be noted that such beneficial effect of seeded growth of ZnO on the grain size has also been demonstrated in the field of low pressure metal-organic chemical vapor deposition by Fanni *et al.* [24].

3.2. Influence of the H_2 plasma on the film properties

The influence of the H_2 plasma treatment on the electrical properties has been determined from Hall measurements. The film resistivity ρ, carrier density N_e and mobility μ as a function of cycle ratio are shown in Fig. 7. Films were either grown without a seed layer, on a 5 nm iZnO seed layer or on a 5 nm seed layer grown with cycle ratio $n=3$.

A few key observations can be made from Fig. 7. When going to lower cycle ratio *n*, the resistivity is observed to decrease, which is due to both an increase in carrier density and in mobility. The increase in carrier density hints at successful doping of the ZnO by H. The increase in carrier mobility most likely stems from both the observed increase in grain size at lower *n*, and the possibility of grain boundary passivation by the embedded H, both reducing the contribution of grain boundary scattering. Interestingly, the carrier mobility is much higher for the

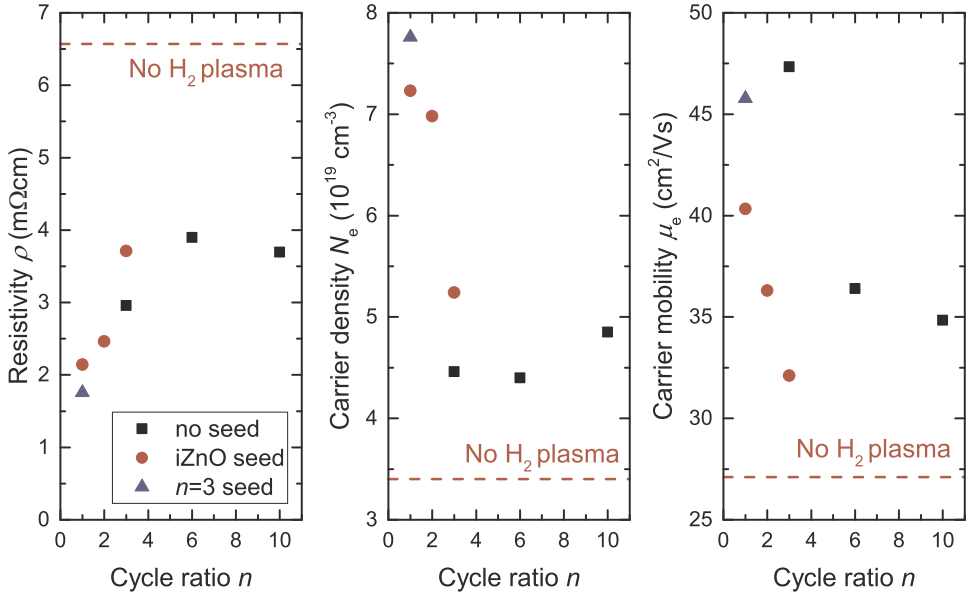

Fig. 7. Resistivity, carrier density and mobility for films prepared using varying cycle ratios (black squares). Films grown on a 5 nm iZnO seed layer are marked by red circles, whereas the film grown on a seed layer grown using $n=3$ is marked by blue triangles.

$n=3$ sample grown without an iZnO seed layer. This directly correlates to the observed reduced grain size when using an iZnO seed layer. Conversely, when comparing the $n=1$ samples grown on either an iZnO or an $n=3$ seed layer, a higher mobility is observed on the $n=3$ seed layer. This is thought to stem from the reduced nuclei density in the $n=3$ seed layer, and hence larger grain size for this sample. This underlines the importance of controlling the initial growth in order to achieve carrier mobility values close to the mobility limit of 55 cm^2/Vs for the carrier density range of these films ($3\times10^{19}-8\times10^{19}$ cm^{-3}) [2].

As also can be seen from Fig. 7, the H_2 plasma is effective in doping the ZnO as the carrier density increases from 3.4×10^{19} cm^{-3} for iZnO to 7.8×10^{19} cm^{-3} for the ZnO:H film grown using a cycle ratio of $n=1^{**}$. The latter condition also gives the most conductive ZnO: H, with a high mobility of 46 cm^2/Vs and a resistivity of 1.8 mΩ cm. It is instructive to compare the results of this work to the aforementioned work of Thomas et al. In that work, much higher carrier density values of up to 4.6×10^{20} cm^{-3} were reported using a very similar approach to grow ALD ZnO: H, albeit at lower carrier mobilities of typically < 20 cm^2/Vs. This shows that in principle higher doping densities can be obtained using H_2 plasmas. Nonetheless, we have explored the parameter space in our system in terms of plasma conditions but were so far not able to achieve a higher doping level. Therefore, it can be speculated that the plasma-doping process is quite dependent on the exact system configuration used, and is likely related to the plasma source configuration. Nonetheless, in both systems (Cambridge Nanotech Fiji 200 ALD system in their case, and an Oxford Instruments OpAL in our case) a remote inductively coupled plasma was used. A table with all the conditions tried in this work as well as resulting film properties can be found in the Supplementary Information.

3.3. Incorporation of H and scattering in ZnO:H films

The incorporation of H in the films by the H_2 plasma treatment has been confirmed using effusion measurements. An iZnO sample and the most conductive sample grown with a cycle ratio $n=1^{**}$ have been studied and the results are shown in Fig. 8. Plotted is the hydrogen effusion rate per cm^2 for films of comparable thickness as a function of temperature. For both materials, an effusion peak near 400 °C is observed followed by an almost constant effusion rate up to highest temperature in case of the iZnO material while for the ZnO:H an effusion maximum near 800 °C is observed. Qualitatively the effusion spectra resemble those of ZnO films grown by LPCVD from DEZ and water vapor and deposited by sputtering, respectively. They were attributed to material with a fairly open structure of grain boundaries in the first case and a more dense material in the second case [25]. The nature of the H effusion peak near 400 °C is not quite clear. For crystalline ZnO, H_2 surface desorption has been reported at temperatures as low as 180 °C [26]. A surface desorption peak near 400 °C was attributed to H diffusing into bulk ZnO and effusing at higher temperature [27]. It might be that the peak arises from rupture of grain boundary related cavities when the pressure of trapped H_2 gets high.

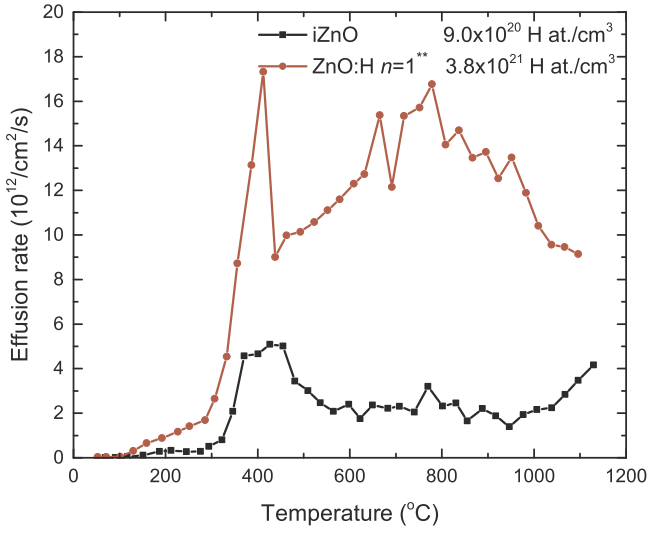

Fig. 8. Effusion rate of hydrogen versus temperature for an iZnO film and our best $n=1^{**}$ ZnO:H film, which consists of a seed layer grown with $n=3$ and subsequently thickened with cycle ratio $n=1$. The total H content in the film, expressed in terms of H at./cm^3 is indicated.

From integration of the calibrated H signal, an atomic H density of 9.0×10^{20} H at./cm^3 and 3.8×10^{21} H at./cm^3 have been found for the iZnO and doped ZnO sample, respectively. We attribute the hydrogen content of the iZnO sample to unintentional H doping during the ALD process, most likely caused by the H_2O reactant. This is much like ALD In_2O_3:H grown from InCp and H_2O/O_2, which is also unintentionally doped by the H_2O reactant [28].

Interestingly, these atomic densities are much higher than what would be needed to account for the observed carrier density, assuming H^+ is the only dopant: only 3.7% of the H in the iZnO sample and 2.0% of the H in the doped sample needs to be active as dopant. Although these seem to be quite low numbers, this is very similar to the value of 3.7% we previously found for crystallized ALD In_2O_3:H. [3] In the case of ALD In_2O_3:H, the inactive H was found to not lead to scattering, since the mobility of the ALD In_2O_3:H was at the mobility limit set by phonon and ionized impurity scattering. Since in this doped film the mobility of 46 cm^2/Vs is quite close to the semi-empirical mobility limit of ~55 cm^2/Vs, it is also expected that inactive H does not lead to strong scattering in ZnO: H.

To further investigate the scattering mechanisms that are limiting the carrier mobility in our films, temperature-dependent Hall measurements have been carried out over a temperature range of 80–350 K. In Fig. 9, the temperature-dependent carrier density and mobility for the iZnO, cycle ratio $n=3$ and cycle ratio $n=1^{**}$ ZnO:H films are shown. As can be seen, for all films the carrier density is independent of the temperature, which is line with their degeneracy. For the iZnO film, a maximum in mobility is found around 260 K, whereas the cycle ratio $n=3$ ZnO:H film has a maximum around 150 K, and a monotonic increase in mobility with decreasing temperature is found for the cycle ratio $n=1^{**}$ ZnO:H film. Also, for both the doped samples, a stronger increase in mobility with decreasing temperature is found. The following can be inferred from these trends: At higher temperatures the mobility is most likely reduced by enhanced phonon scattering. Since the doped samples experience a stronger decrease at higher temperatures, the mobility of these films is thought to be relatively more limited by phonon scattering. This is line with their mobility values being closer to the mobility limit. The decrease in carrier mobility at lower temperatures observed for the iZnO and cycle ratio $n=3$ ZnO:H films points to transport being limited by thermionic emission across grain boundaries. The fact that the maximum in mobility occurs at lower temperatures for the cycle ratio $n=3$ film than for the iZnO film can be explained by a reduced contribution of grain boundary scattering, both by the enhanced grain size and possibly a reduced barrier height at the grain boundary by passivation with H. Note that it was attempted to fit the mobility curves using existing models for temperature-dependent carrier transport across grain boundaries, phonon scattering and ionized impurity scattering in order to extract their relative contributions to the total scattering and the barrier height for thermionic emission over the grain boundaries. Unfortunately, although satisfactory fits could be obtained, the solutions were found not to be unique.

3.4. Comparison to other TCOs and prospects for solar cell applications

In the foregoing it has been shown how high mobility (47 cm^2/Vs) ZnO:H with a resistivity of 1.8 mΩcm can be prepared by ALD. In this

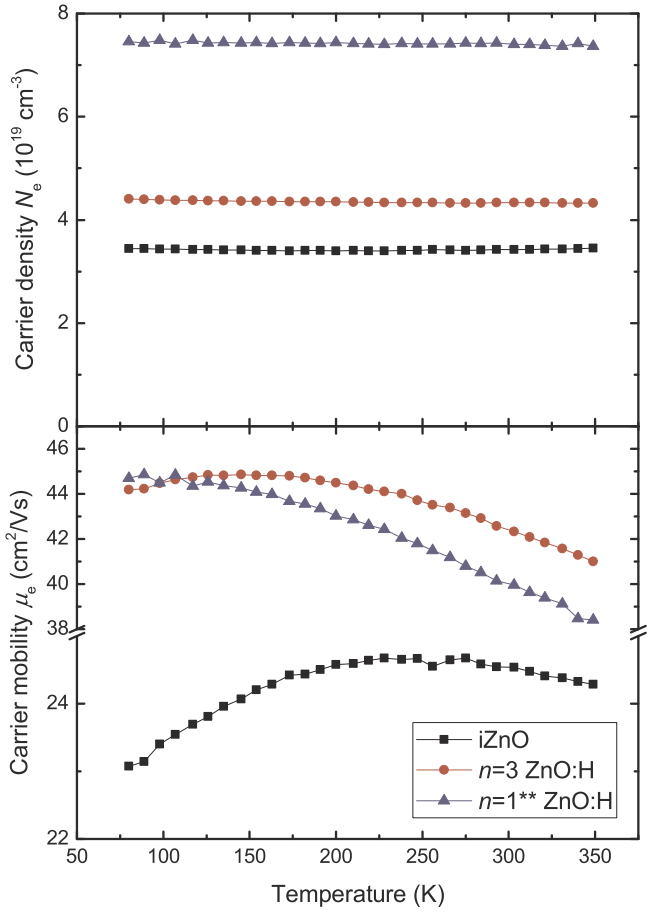

Fig. 9. Temperature-dependent carrier density N_e (top panel) and carrier mobility μ_e (bottom panel) of an iZnO film, a $n=3$ and a $n=1^{**}$ ZnO:H film.

section, the developed ZnO:H is compared to other TCO materials in terms of electrical properties and spectral absorption coefficient. Also, the potential of the developed ZnO:H for various Si heterojunction configurations is discussed.

The electrical properties and absorption coefficient of ITO, In_2O_3:H, ZnO, ZnO:B, ZnO:Al and ZnO:H are compared in Table 1 and Fig. 10, respectively. As can be seen, the best film grown with the H_2 plasma treatment has a sheet resistance of 237 Ω/sq. This is a strong improvement over the sheet resistance of 903 Ω/sq for an ALD iZnO film, and this improvement is due to the strong increase in both carrier mobility and carrier density. Despite the higher mobility, the sheet resistance of ZnO:H is still higher than for Al- and B-doped ZnO due to the much lower doping level of ZnO:H. However, the low doping level and high mobility of ZnO:H lead to very promising optical properties: Compared to Al- and B-doped ZnO, ZnO:H has negligible free carrier absorption and a lower bandgap. Both can be explained by the lower

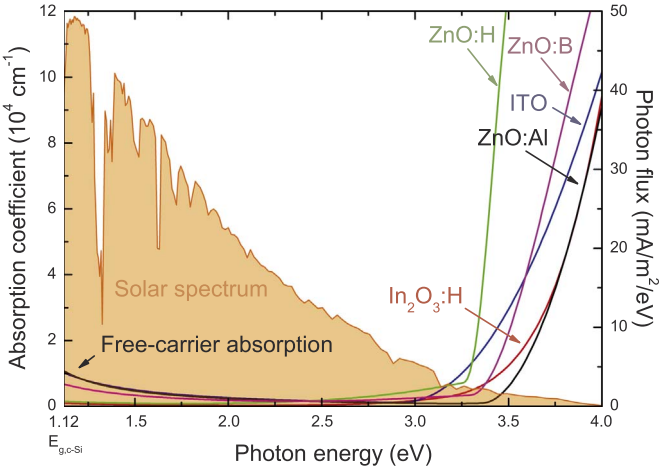

Fig. 10. Absorption coefficient for various TCOs as listed in Table 1. For reference, the photon flux in the AM1.5 g spectrum is shown as well.

carrier density of ZnO:H, which leads to a smaller Drude contribution and less widening of the optical band gap through the so-called Burstein-Moss shift [29].

When assessing the potential of the developed ZnO:H film for SHJ solar cell applications, it is important to consider that TCOs are used in different configurations in these types of cells, which lead to different requirements for the TCO. When applied as the front contact electrode of SHJ cells, the TCO should be ~75 nm thick for antireflection purposes, have little FCA and FCR to enable a high J_{sc}, and have a sufficiently low sheet resistance to avoid *FF* losses. Holman et al. observed significant fill factor reductions in SHJ solar cells for front TCO sheet resistance values exceeding 100 Ω/sq, although this is of course dependent on the exact metal grid design. [31] At the rear side, the TCO is usually thicker (> 100 nm) and thus has a less stringent resistivity requirement, whereas the sheet resistance does not play a role when full area metallization is applied. Also, especially at the rear side a good performance in the NIR is desired, since it is mostly the low-energy photons that make it to the rear of the cell. [32] On the other hand, in a c-Si/perovskite tandem cell the bottom c-Si cell should be tuned to the NIR as much as possible, making it prerequisite that the front TCO does not have a strong Drude contribution. [33] In addition, since the current in a tandem cell is lower, the sheet resistance can be about three times higher compared to a single junction SHJ solar cell for an equal ohmic power loss. [33] Finally, the formation of a proper electrical contact between the TCO and both the carrier-selective layers and metallization should be verified.

Looking at Table 1, the sheet resistance of 75 nm of ZnO:H of 237 Ω/sq seems to be too high for application as front TCO in a SHJ cell. Nonetheless, its optical performance would be very good. In Table 1, the expected J_{sc} when using these TCOs in SHJ solar cells with a conventional 5 nm a-Si: H(i)/10 nm a-Si: H(p)/75 nm TCO front contact has been simulated with OPAL 2, using the optical constants of

Table 1
Electrical properties and simulated J_{sc} of a SHJ solar cell with the various TCOs at the front side. Simulations were performed with OPAL2. All TCOs were ~75 nm thick. The In_2O_3:H sample was prepared at 100 °C and post-deposition crystallized at 200 °C. All ALD ZnO TCOs were prepared at 200 °C [22,30].

TCO	Deposition technique	Dopant precursor	Cycle ratio n	μ_e (cm^2/Vs)	N_e (10^{20} cm^{-3})	R_s (Ω/sq)	J_{sc} (mA/cm^2)
ITO [22]	Sputtering	ITO target	–	36	5.3	53	39.6
In_2O_3:H	ALD	H_2O	–	138	1.6	36	40.7
iZnO	ALD	–	–	27	0.3	903	40.6
ZnO:Al	ALD	DMAI	10[a]	13	7.0	93	37.8
ZnO:B	ALD	TIB	15[b]	16	4.1	133	39.3
ZnO:H	ALD	H_2 plasma	1^{**}	46	0.8	237	40.5

[a] 10 cycles of ALD ZnO, followed by 1 cycle of dimethylaluminum isopropoxide (DMAI) and H_2O.
[b] 15 cycles of ALD ZnO, followed by 1 cycle of triisopropyl borate (TIB) and H_2O.

the TCOs as determined from spectroscopic ellipsometry as input. [34] The optical constants of the a-Si:H layers were taken from the work of Holman et al. [31] As can be seen, for ZnO:H a very high J_{sc} is obtained from the simulation, close to the best In_2O_3:H, mainly due to the high mobility and lower carrier density which lead to negligible FCA and FCR. Yet, for application as a front TCO, a further reduction in the resistivity of the ZnO:H should be targeted by enhancing the doping level. This could either be pursued by further optimization of the H_2 plasma treatment, or by enhancing the carrier density by co-doping using Al or B dopants, thereby benefiting simultaneously from the enhanced grain size induced by the H_2 plasma and the higher doping level that is easily achievable with these classical dopants.

For application as rear TCO in a bifacial SHJ cell, the resistivity of ZnO:H seems to be around the required value, whereas its resistivity does not play a role for a SHJ cell with full rear metallization. In terms of optical potential, the excellent optical performance in the NIR of ZnO:H should make it highly suited as rear optical spacer for such cells. Finally, the ALD ZnO:H seems very suitable for use as TCO in a c-Si/perovskite tandem cell: due to the reduced current in such cells the sheet resistance of 237 Ω/sq is adequate. In addition, the excellent performance in the NIR of ALD ZnO:H nicely aligns with the requirement of a NIR-tuned bottom c-Si cell in such tandems.

4. Conclusions

In this work, high-mobility ZnO:H films have been prepared using thermal ALD of ZnO in conjunction with H_2 plasma treatments. It has been shown that by choosing a deposition regime in which film growth and etching by the H_2 plasma are in strong competition can lead to a strong increase in grain size and associated enhancement of the mobility to values as high as 47 cm^2/Vs. Besides increasing the grain size, the H_2 plasma is able to dope the ZnO:H to an intermediate doping level of 8×10^{19} cm^{-3}, and a minimum in resistivity of 1.8 mΩ cm has been reached. The successful incorporation of H in the film has been corroborated by effusion measurements, and temperature-dependent Hall measurements suggest that grain boundary scattering is strongly reduced in ZnO:H. In a comparison with other ZnO- and In_2O_3-based materials it has been shown that ZnO:H exhibits excellent NIR-transparency, but that the resistivity of ZnO:H is higher due to its lower carrier density. Finally, the application of ALD ZnO:H as TCO in SHJ solar cells has been discussed and it has been shown that ZnO:H has promising properties to be used as rear TCO in SHJ cells as well as front TCO in SHJ-perovskite tandem cells.

Acknowledgements

The authors acknowledge J. J. L. M. Meulendijks, C. O. van Bommel, C.A.A. van Helvoirt, J. van Gerwen and J. J. A. Zeebregts for their technical support. The authors gratefully acknowledge Solliance for funding the TEM facility. Dr. Bas W.H. van de Loo is acknowledged for fruitful discussions. R.J. van Gils is thanked for providing the schematic of the OpAL system. This research has received funding from the European Union's Horizon 2020 research and innovation programme under grant agreement No. 641864 (INREP). Further, we acknowledge financial support for this research from the Top consortia for Knowledge and Innovation (TKI) Solar Energy programs “COMPASS” (TEID215022) and “RADAR” (TEUE116905) of the Ministry of Economic Affairs of The Netherlands.

Appendix A. Supplementary material

Supplementary data associated with this article can be found in the online version at http://dx.doi.org/10.1016/j.solmat.2017.05.040.

References

[1] B. Macco, B.W.H. van de Loo, W.M.M. Kessels, Atomic Layer Deposition for High Efficiency Crystalline Silicon Solar Cells, Wiley, 2017.
[2] K. Ellmer, R. Mientus, Carrier transport in polycrystalline transparent conductive oxides: a comparative study of zinc oxide and indium oxide, Thin Solid Films. 516 (2008) 4620–4627, http://dx.doi.org/10.1016/j.tsf.2007.05.084.
[3] B. Macco, H.C.M. Knoops, W.M.M. Kessels, Electron Scattering and Doping Mechanisms in Solid-Phase-Crystallized In_2O_3:H Prepared by Atomic Layer Deposition, ACS Appl. Mater. Interfaces 7 (2015) 16723–16729, http://dx.doi.org/10.1021/acsami.5b04420.
[4] S. De Wolf, A. Descoeudres, Z.C. Holman, C. Ballif, High-efficiency Silicon Heterojunction Solar Cells: a Review, Green 2 (2012) 7–24, http://dx.doi.org/10.1515/green-2011-0018.
[5] T. Koida, M. Kondo, K. Tsutsumi, A. Sakaguchi, M. Suzuki, H. Fujiwara, Hydrogen-doped In_2O_3 transparent conducting oxide films prepared by solid-phase crystallization method, J. Appl. Phys. 107 (2010) 33514, http://dx.doi.org/10.1063/1.3284960.
[6] B. Macco, Y. Wu, D. Vanhemel, W.M.M. Kessels, High mobility In_2O_3:H transparent conductive oxides prepared by atomic layer deposition and solid phase crystallization, Phys. Status Solidi - Rapid Res. Lett. 8 (2014) 987–990, http://dx.doi.org/10.1002/pssr.201409426.
[7] J. Yu, J. Bian, W. Duan, Y. Liu, J. Shi, F. Meng, Z. Liu, Tungsten doped indium oxide film: ready for bifacial copper metallization of silicon heterojunction solar cell, Sol. Energy Mater. Sol. Cells 144 (2016) 359–363, http://dx.doi.org/10.1016/j.solmat.2015.09.033.
[8] Y. Yoshida, D.M. Wood, T.A. Gessert, T.J. Coutts, High-mobility, sputtered films of indium oxide doped with molybdenum, Appl. Phys. Lett. 84 (2004) 2097–2099, http://dx.doi.org/10.1063/1.1687984.
[9] L. Barraud, Z.C. Holman, N. Badel, P. Reiss, A. Descoeudres, C. Battaglia, S. De Wolf, C. Ballif, Hydrogen-doped indium oxide/indium tin oxide bilayers for high-efficiency silicon heterojunction solar cells, Sol. Energy Mater. Sol. Cells 115 (2013) 151–156, http://dx.doi.org/10.1016/j.solmat.2013.03.024.
[10] Y. Kuang, B. Macco, B. Karasulu, C.K. Ande, P.C.P. Bronsveld, M.A. Verheijen, Y. Wu, W.M.M. Kessels, R.E.I. Schropp, Towards the implementation of atomic layer deposited In_2O_3:H in silicon heterojunction solar cells, Sol. Energy Mater. Sol. Cells 163 (2017) 43–50, http://dx.doi.org/10.1016/j.solmat.2017.01.011.
[11] B. Macco, M.A. Verheijen, L.E. Black, B. Barcones, J. Melskens, W.M.M. Kessels, On the solid phase crystallization of In_2O_3:H transparent conductive oxide films prepared by atomic layer deposition, J. Appl. Phys. 120 (2016) 85314, http://dx.doi.org/10.1063/1.4962008.
[12] C.G. Van De, Walle, Hydrogen as a cause of doping in zinc oxide, Phys. Rev. Lett. 85 (2000) 1012–1015 ⟨http://www.ncbi.nlm.nih.gov/pubmed/10991462⟩.
[13] X.-B. Li, S. Limpijumnong, W.Q. Tian, H.-B. Sun, S.B. Zhang, Hydrogen in ZnO revisited: bond center versus antibonding site, Phys. Rev. B. 78 (2008) 113203, http://dx.doi.org/10.1103/PhysRevB.78.113203.
[14] B.L.L. Zhu, J. Wang, S.J.J. Zhu, J. Wu, R. Wu, D.W.W. Zeng, C.S.S. Xie, Influence of hydrogen introduction on structure and properties of ZnO thin films during sputtering and post-annealing, Thin Solid Films. 519 (2011) 3809–3815, http://dx.doi.org/10.1016/j.tsf.2011.01.187.
[15] M.A. Thomas, J.C. Armstrong, J. Cui, New approach toward transparent and conductive ZnO by atomic layer deposition: hydrogen plasma doping, J. Vac. Sci. Technol. A Vac., Surf., Film. 31 (2013) 01A130, http://dx.doi.org/10.1116/1.4768172.
[16] M.D. McCluskey, S.J. Jokela, K.K. Zhuravlev, P.J. Simpson, K.G. Lynn, Infrared spectroscopy of hydrogen in ZnO, Appl. Phys. Lett. 81 (2002) 3807–3809, http://dx.doi.org/10.1063/1.1520703.
[17] J.J. Dong, X.W. Zhang, J.B. You, P.F. Cai, Z.G. Yin, Q. An, X.B. Ma, P. Jin, Z.G. Wang, P.K. Chu, Effects of hydrogen plasma treatment on the electrical and optical properties of ZnO films: identification of hydrogen donors in ZnO, ACS Appl. Mater. Interfaces 2 (2010) 1780–1784, http://dx.doi.org/10.1021/am100298p.
[18] L. Ding, S. Nicolay, J. Steinhauser, U. Kroll, C. Ballif, Relaxing the conductivity/transparency trade-off in MOCVD ZnO thin films by hydrogen plasma, Adv. Funct. Mater. 23 (2013) 5177–5182, http://dx.doi.org/10.1002/adfm.201203541.
[19] D. Gaspar, L. Pereira, K. Gehrke, B. Galler, E. Fortunato, R. Martins, High mobility hydrogenated zinc oxide thin films, Sol. Energy Mater. Sol. Cells 163 (2017) 255–262, http://dx.doi.org/10.1016/j.solmat.2017.01.030.
[20] H.C.M. Knoops, B.W.H. van de Loo, S. Smit, M.V. Ponomarev, J.-W. Weber, K. Sharma, W.M.M. Kessels, M. Creatore, Optical modeling of plasma-deposited ZnO films: electron scattering at different length scales, J. Vac. Sci. Technol. A Vac., Surf., Film. 33 (2015) 21509, http://dx.doi.org/10.1116/1.4905086.
[21] W. Beyer, F. Einsele, Hydrogen Effusion Experiments, in: D. Abou-ras, T. Kirchartz, U. Rau (Eds.), Adv. Charact. Tech. Thin Film Sol. Cells, Wiley, 2011, pp. 569–595.
[22] B. Macco, D. Deligiannis, S. Smit, R.A.C.M.M. van Swaaij, M. Zeman, W.M.M. Kessels, Influence of transparent conductive oxides on passivation of a-Si:H/c-Si heterojunctions as studied by atomic layer deposited Al-doped ZnO, Semicond. Sci. Technol. 29 (2014) 122001, http://dx.doi.org/10.1088/0268-1242/29/12/122001.
[23] Y. Wu, P.M. Hermkens, B.W.H. van de Loo, H.C.M. Knoops, S.E. Potts, M.A. Verheijen, F. Roozeboom, W.M.M. Kessels, Electrical transport and Al doping efficiency in nanoscale ZnO films prepared by atomic layer deposition, J. Appl. Phys. 114 (2013) 24308, http://dx.doi.org/10.1063/1.4813136.
[24] L. Fanni, A.B. Aebersold, M. Morales-Masis, D.T.L. Alexander, A. Hessler-Wyser, S. Nicolay, C. Hébert, C. Ballif, Increasing Polycrystalline Zinc Oxide Grain Size by Control of Film Preferential Orientation, Cryst. Growth Des. 15 (2015) 5886–5891,

http://dx.doi.org/10.1021/acs.cgd.5b01299.
[25] W. Beyer, U. Breuer, F. Hamelmann, J. Hüpkes, A. Stärk, H. Stiebig, U. Zastrow, Hydrogen Diffusion in Zinc Oxide Thin Films, MRS Proceedings 1165 1165-M05-24. http://dx.doi.org/10.1557/PROC-1165-M05-24, 2009.
[26] W.H. Doh, P.C. Roy, C.M. Kim, Interaction of hydrogen with ZnO: surface adsorption versus bulk diffusion, Langmuir 26 (2010) 16278–16281, http://dx.doi.org/10.1021/la101369r.
[27] P.C. Roy, W.H. Doh, S.K. Jo, C.M. Kim, Interaction of methanol and hydrogen on a ZnO (0001) single crystal surface, J. Phys. Chem. C. 117 (2013) 15116–15121, http://dx.doi.org/10.1021/jp403913h.
[28] Y. Wu, B. Macco, D. Vanhemel, S. Kölling, M.A. Verheijen, P.M. Koenraad, W.M.M. Kessels, F. Roozeboom, Atomic Layer Deposition of In_2O_3:H from InCp and H_2O/O_2: microstructure and Isotope Labeling Studies, ACS Appl. Mater. Interfaces 7 (2016), http://dx.doi.org/10.1021/acsami.6b13560.
[29] E. Burstein, Anomalous Optical Absorption Limit in InSb, Phys. Rev. 93 (1954) 632–633, http://dx.doi.org/10.1103/PhysRev.93.632.
[30] D. Garcia-Alonso, S.E. Potts, C.A.A. van Helvoirt, M.A. Verheijen, W.M.M. Kessels, Atomic layer deposition of B-doped ZnO using triisopropyl borate as the boron precursor and comparison with Al-doped ZnO, J. Mater. Chem. C. 3 (2015) 3095–3107, http://dx.doi.org/10.1039/C4TC02707H.
[31] Z.C. Holman, A. Descoeudres, L. Barraud, F.Z. Fernandez, J.P. Seif, S. De Wolf, C. Ballif, Current Losses at the Front of Silicon Heterojunction Solar Cells, IEEE J. Photovolt. 2 (2012) 7–15, http://dx.doi.org/10.1109/JPHOTOV.2011.2174967.
[32] Z.C. Holman, M. Filipič, A. Descoeudres, S. De Wolf, F. Smole, M. Topič, C. Ballif, Infrared light management in high-efficiency silicon heterojunction and rear-passivated solar cells, J. Appl. Phys. 113 (2013) 13107, http://dx.doi.org/10.1063/1.4772975.
[33] B. Chen, Y. Bai, Z. Yu, T. Li, X. Zheng, Q. Dong, L. Shen, M. Boccard, A. Gruverman, Z. Holman, J. Huang, Efficient Semitransparent Perovskite Solar Cells for 23.0%-Efficiency Perovskite/Silicon Four-Terminal Tandem Cells, Adv. Energy Mater. 6 (2016) 1–7, http://dx.doi.org/10.1002/aenm.201601128.
[34] K.R. McIntosh, S.C. Baker-Finch, OPAL 2: Rapid optical simulation of silicon solar cells, in: 2012 38th IEEE Photovolt. Spec. Conference, IEEE: pp. 000265–000271. doi:http://dx.doi.org/10.1109/PVSC.2012.6317616, 2012.